Evaluation of Computed Tomography Techniques for Material Identification in Low Level and Intermediate Level Waste. 16648

Stephen Halliwell, VJ Technologies Inc, 89 Carlough Road, Bohemia, NY 11716, USA.
Apostolos Christodoulou, VJ Technologies Europe, Z.I. de la Forêt, Rue Jules Guesde, 91860 Epinay-sous-Sénart, France

INTRODUCTION

Measures required to assure long term safe storage of Low-level and intermediate-level short-lived (LIL/SL) waste generated by the nuclear-power industry in France include the characterization of the waste and identification of materials within the waste.

Digital Radiography (DR) techniques using x-ray at energies in the 6MeV range have been shown to be effective for validation of the integrity of the concrete containers, and it was considered that the use of this technique together with the addition of Computed Tomography (CT) techniques could effectively identify materials within the waste.

This paper describes the initial evaluation of two DR imaging techniques and two CT techniques using x-ray energy spectra up to 9MeV to inspect a surrogate waste package, which comprised an outer concrete cylindrical container of 1400mm diameter with 148mm wall thickness, and an overall volume of 2 meters cubed, within which a 200 liter drum containing representative heterogeneous inactive waste, was placed in the center and the annulus between the 200 liter drum and the outer cylindrical package was filled with cement grout. The surrogate waste within the 200 liter drum comprised three separate layers of high density, medium density and low density mixed materials.

The equipment used was a linear accelerator producing high energy spectra at either 6MeV or 9MeV and a high-precision CT manipulator with X, Y, Z and rotation motions, which were common to all techniques investigated. Two different digital detectors were used in the DR and CT performance evaluations, a Digital Detector Array (DDA) comprising a columnar Thallium-doped Cesium-Iodide scintillator screen in intimate contact with a 2k by 2k array of amorphous silicon detectors, 200µm x 200µm in area, and a Linear Diode Array (LDA) comprising a line of Cadmium-Tungstate columns, 1cm thick and 400µm x 400µm in area.

The work comprised evaluations of linear accelerator spectra and the attenuation effects of the waste container and contents, image acquisition performance of each detector, and CT techniques using area detector and linear detector. The results presented in this paper include mathematical evaluation of the two CT techniques, and analysis of measurement data, digital images, CT reconstruction images, and

estimated material densities. The data was compared with recorded details and photographs of the actual configuration of materials within the surrogate waste.

The Digital Detector Array can generate CT inspection volumes with considerable resolution and detail for the low-density and medium-density sections of the surrogate waste, however, the high-density sections were not imaged with sufficient detail and the images contained a large number of artifacts mainly due to the detectors lack of high energy photon stopping power. Materials identification with the Digital Detector Array, while possible for certain materials, for materials in the steel to plastic density range the attenuation values of the voxels in the reconstruction are too similar and difficult to resolve from the artifacts present.

The Linear Diode Array can generate CT inspection volumes of regions of interest of the low-density and medium-density sections with considerable resolution and contrast, and potentially acceptable levels of resolution and contrast of the high-density section of the waste. While a few artifacts were present in the reconstructions, the majority are not due to the fundamental properties of the detector and are considered to be correctable. Materials identification with the LDA inspection data appear to be viable, with steel, copper, and higher-density metals being readily be distinguished from other materials on the basis of voxel value.

Future work is needed to obtain a better definition of optimum spatial resolution and inspection speed, and to develop a system of "calibration rods which would consist of a series of 50mm diameter cylinders of 7 materials; Plastic, Teflon, Concrete, Aluminum, Copper, Tungsten and Lead. The cylinders will be distributed at a certain radius in the surrogate waste and will be used as reference points in the evaluation and demonstration of the contrastive performance for the low, medium and high-density cases.

The ability to identify the materials within a sealed waste container, by non-destructive examination, enables the verification of waste acceptance criteria without the need to open the waste containers. This eliminates the need for complex and expensive equipment to open and remotely handle the intermediate level waste, avoids potential hazards and risk of personnel dose uptake, and does not increase the volume of waste caused by repackaging of materials after examination and the decontamination or disposal of equipment used.

EQUIPMENT USED IN THE TESTS

These tests were made in the high energy laboratory of VJ Technologies (VJT), at their East Haven, Connecticut site.

Figure 1 – VJT High Energy facility located at East Haven Connecticut.

High Energy X-Ray Source
The high energy x-ray source used in the tests was a VARIAN M9A model which can produce high energy spectra at 6MeV and 9MeV. This is shown in Figure 2.

Figure 2 – VARIAN M9A LINATRON

Digital Detector Array
The Digital Detector Array used was a Perkin-Elmer, PE1620 model, with a 40cm x 40cm active area, reduced to about 36.5cm x 36.5cm by the extra-shielding around the electronics to prevent damage due to radiation. Detector pixel pitch was 0.2mm and the detector has a columnar Thallium-doped Cesium-Iodide (CSITl) scintillator screen in intimate contact with a 2k by 2k array of 0.2mm amorphous silicon detectors. Digitization for this detector can be as high as 16-bits.

Linear Diode Array
The Linear Diode Array detector has a 0.4mm pixel pitch, with 1024 elements. The scintillators for the detectors were 1.0cm columns of Cadmium-Tungstate (CdWO4) Detector digitization was at 16-bits.

The tomography hardware with the Digital Detector Array is shown in Figure 3. The manipulator includes 4 independent axes: X, Y, Z and rotation. The manipulator

has a high-precision turntable, which can handle up to 4,545 kg, and specially designed to acquire tomography data.

The detectors and the high energy x-ray source were at a source to detector distance of 4,369mm, with travel of +/- 1,100mm on the X-axis, 1,000mm maximum travel on the vertical Y axis and continuous 360 degree of rotation with the rotary axis.

Figure 3 – Tomography hardware with the digital detector array.

The software used for the acquisition and treatment of the images, and control of the mechanical equipment of the tomography manipulator to support a variety of scanning modalities is Vi3, from VJ Technologies.

Figure 4 includes sketches of some the scanning modalities available as options.

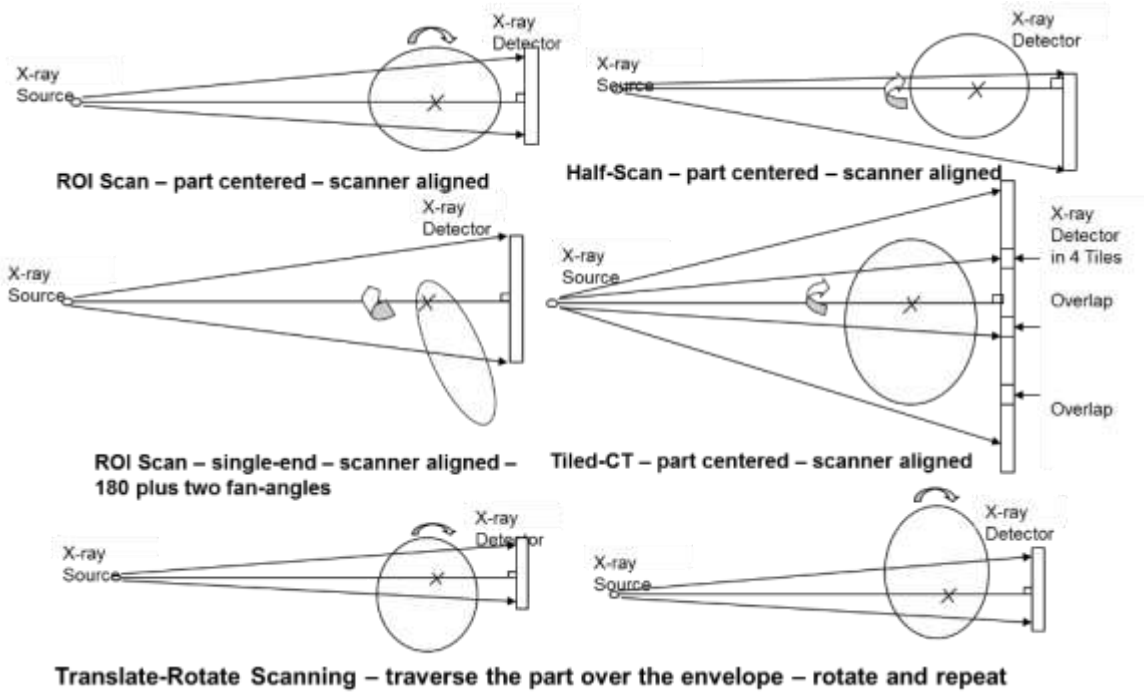

Figure 4 – Scanning options for acquiring CT inspection data

CONTAINER USED IN TESTS

The test container comprised a 200 liter drum into which was placed 3 plastic bins filled with surrogate waste separated into low, medium and high density by each drum. The 200 liter drum was placed in a concrete cask, as shown in Figure 5, and the void filled with cement based grout.

The total weight of the test container was 3,928kg.

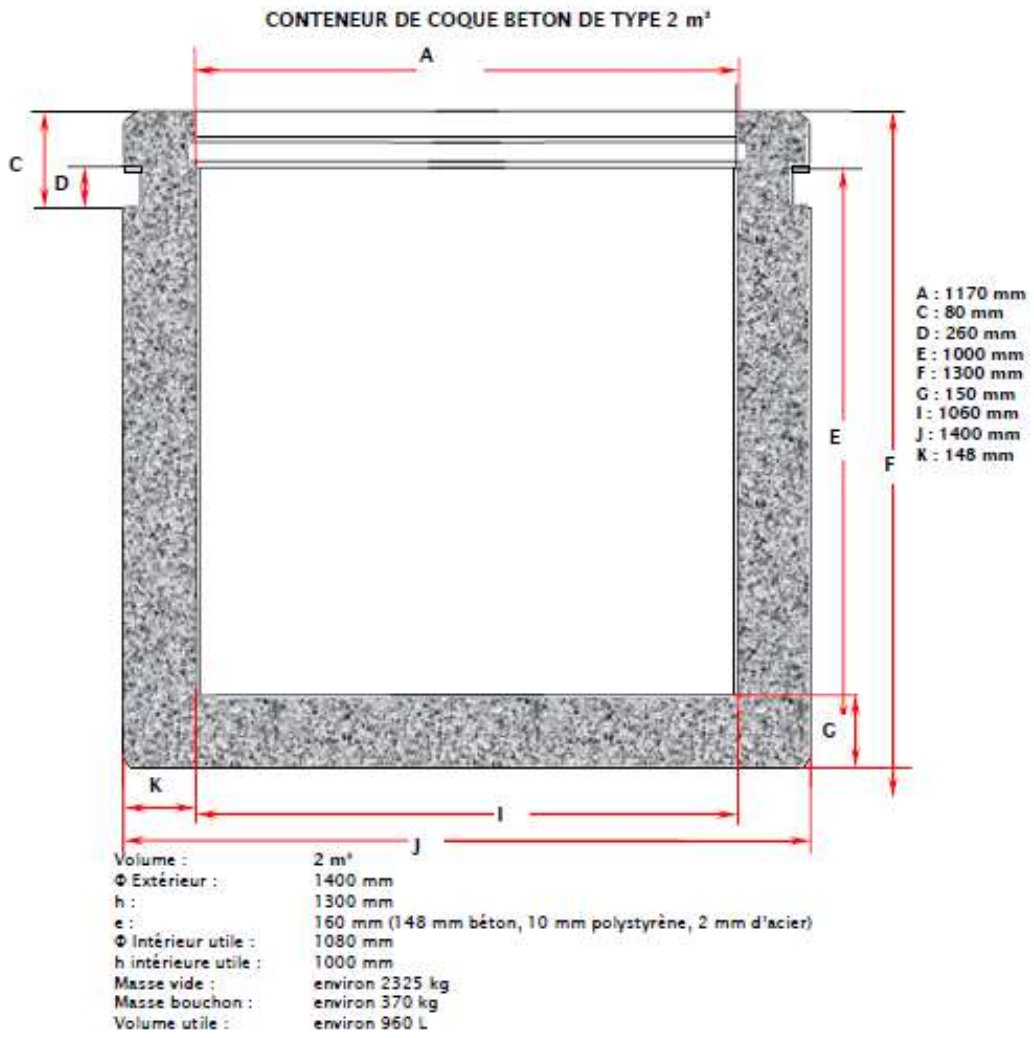

Figure 5 – Drawing of the Concrete Cask built for these tests

DISCUSSION OF X-RAY SPECTRA AND PERFORMANCE OF DETECTORS

The challenges for CT inspection in this context derive from the substantial attenuation due to the container, the material and the shape, which determines the energy range available for the inspection of the contents of the inner drum. Figure 6 includes a plot of a normalized 9 MeV spectrum, and the same spectra after attenuation through the center of the Concrete container.

In addition, type of CT data acquisition described in this paper, the exact state of the spectrum will change with horizontal position of the detector panel – as acquisition towards the tangents of the concrete cylinder will be much more attenuating than through the center of the cylinder.

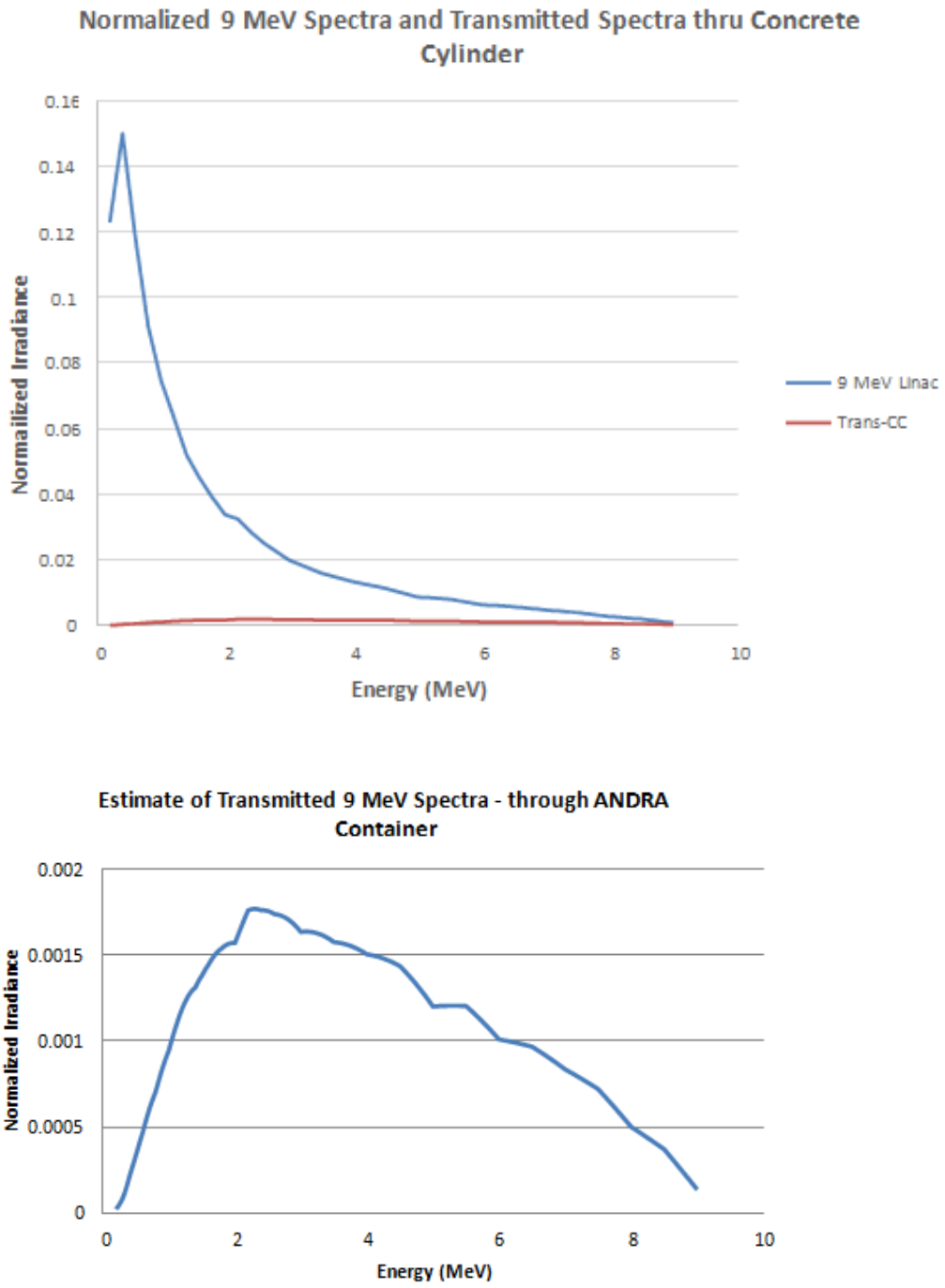

Figure 6 – Estimated 9 MeV LINAC spectra and spectra after transmission through ANDRA container.

This plot of spectra did not include the use of an x-ray beam filter. In describing the problem, it was considered best to leave the choice of filter open. Filter selection varied for the different chord lengths through the drum and the specific detector used.

In general, to get more detail, a lower average energy is required, whereas to reduce artifacts a higher average energy is required.

The concrete container serves to increase the average energy for the inspection of the inner contents in the drum. This physical circumstance has two impacts. First, imaging in this context requires a thicker detector which can stop-and-count the higher average energy. Secondly, contrastive performance for differences in materials scales to their attenuation value at MeV energies, where the predominant attenuation mechanisms are Compton scattering, and for higher-Z materials Pair production. The result is material differences that will scale with the density of the materials, and have little to do with atomic number independent of density. Table 1 includes some x-ray attenuation values for assorted materials at 3MeV.

Material	Attenuation (cm-1)	mm-1
Plastic	0.05761	(0.00576 mm-1)
Concrete	0.0843	(0.00843 mm-1)
Aluminum	0.0956	(0.00956 mm-1)
Steel	0.2822	(0.02822 mm-1)
Brass	0.3187	(0.03187 mm-1)
Copper	0.3223	(0.03223 mm-1)
Lead	0.4727	(0.04727 mm-1)

Table 1 – Attenuation values for materials at 3 MeV

As can be seen from the table, at this energy, the system contrastive performance requirements vary with type of materials. The scanner contrastive properties for sorting Lead from Plastic, or Concrete to Air, are less than sorting Aluminum from Concrete, or say Plastic from Rubber. In addition, from the geometry of the cylinder the transmitted spectrum will vary over the projected area of the detector and the different rates of x-ray transmission for the different acquisitions in the 'Tiled- CT', 'Range-Extended CT', or 'Region of Interest' (ROI) CT scanning will have to be accounted for.

In this context, ROI scanning, included a number of advantages. One goal of this inspection was the material identification for the contents of the 200 liter Drum. Achieving this goal required more spatial resolution and contrast than necessary for the inspection of the outer concrete cylinder or other items. Scanning the entire assembly, concrete cylinder included, required substantially more time. For these reasons it was decided to the implement ROI for the investigation.

The Digital Detector Array had a 1mm Cesium-Iodide Thallium- Doped scintillator (Density ~ 5gm/cc). The Linear Detector Array had 1cm Cadmium-Tungstate scintillator crystals. Figure 7 shows plots of the relative difference in stopping power for different scintillators for the transmitted 9 MeV spectrum.

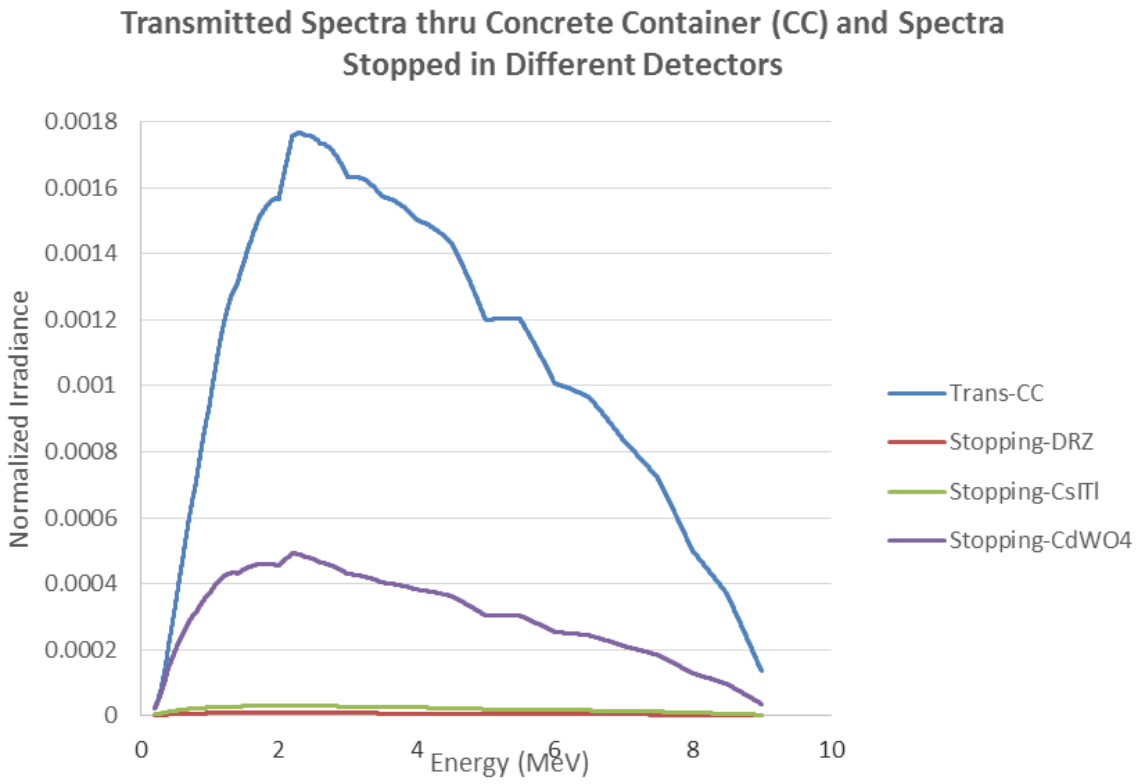

Figure 7 – Transmitted 9 MeV spectra and comparison of stopping power for different scintillators.

Notice the much reduced stopping power in the 1mm CsITl as compared to the 1cm CdWO4 scintillator. This results in a higher contrast sensitivity being achieved by the Linear Diode Array, but better spatial resolution and overall faster scanning being achieved by the Digital Detector Array.

TOMOGRAPHY WITH THE DIGITAL DETECTOR ARRAY

As this was an area detector, cone-beam scanning and reconstruction techniques were used to generate CT volumetric data. Figure 8 illustrates the scanning geometry, showing how an entire section of the cone-beam of irradiance from the x-ray source illuminates the areal detector. In this case the concrete cask is rotated, and moved horizontally and vertically to enable the detector to cover the x-ray projection of the entire object.

The Translate-Rotate scanning technique illustrated in Figure 5 was used to acquire data.

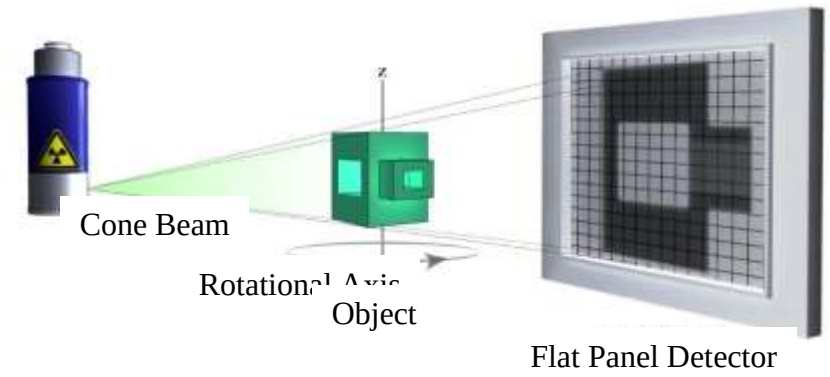

3D Cone Beam Geometry

Figure 8 – Illustration of Cone-Beam CT geometry

All the acquisitions were performed with a 9MeV linear accelerator at maximum power and a detector integration time of 5 seconds. Four acquisitions at 400 to 800 views were acquired. Acquisition times varied from 4.5 hours to 18.5 hours.

Figure 9 –Concrete Cask in position for data acquisition for translate-rotate scanning

Figure 9 shows the hardware for the Digital Detector Array data acquisition. The source to object distance was 3,327.4mm resulting in an x-ray magnification of 1.31.

The input data to CT reconstruction is 'attenuation measurements' – where the 'transmission data' is converted via a subtraction of the 'reference irradiance' in the natural-log scale (equivalent to dividing by the reference irradiance then taking the natural log). Equations below show one parametrization of the transmission (T) and attenuation measurements (A). The point here is – a measurement of the 'reference irradiance' is a key component in the CT acquisition process – and is part of the calculation of every input pixel to the CT reconstruction algorithm.

$$T\left[S(E),\bar{Z},\bar{\rho},y_\ell\right]=\frac{\Phi^P\left[S(E),\bar{Z},\bar{\rho},y_\ell\right]}{\int\Phi_0^P\left[S(E)\right]dE}\approx\int e^{-\sum_i^n\mu_m^i\left[S(E),Z_i\right]\rho_i y_\ell^i}dE$$

Where $T(E,Z,\rho,y_\ell)$ is transmission, and

$$A(E,Z,\rho,y_\ell)\quad=\quad\ln\left(\frac{\int\Phi_0^P\left[S(E)\right]dE}{\Phi^P\left[S(E),\bar{Z},\bar{\rho},y_\ell\right]}\right)\approx\sum_i^n\mu_m^i\left(\bar{E},Z_i\right)\rho_i y_\ell^i$$

Where $A(E,Z,\rho,y_\ell)$ represents the attenuation, and $\int\Phi_0^P[S(E)$ dE, represents the reference irradiance integrated over the source spectrum, and μ represents total linear attenuation. In the table the units are inverse centimeters (cm-1). Since the pixel sizes were in mm, the units for reconstruction are in inverse millimeters (mm-1).

In this imaging context it was not feasible to acquire a measure of the reference irradiance in the usual way, the difference in irradiance with no Concrete Cask in the field of view, and the irradiance with the Concrete Cask in the field of view since that was larger than the dynamic range of the detector.

Consequently, the values of the 'reference irradiance' were estimated from a range of measurements of the empty container. This estimation process, however, results in the generation of artifacts in the images.

The CT results were then reviewed for each of the three types of waste, high, medium and low, density. Figure 10 shows a photo of the high density waste.

Figure 10 –High-Density section of the drum

Figure 11 shows a vertical slice through the high density waste, with 4 locations identified as A, B, C and D. Horizontal slices at each location are shown in Figures 12, 13, 14 and 15.

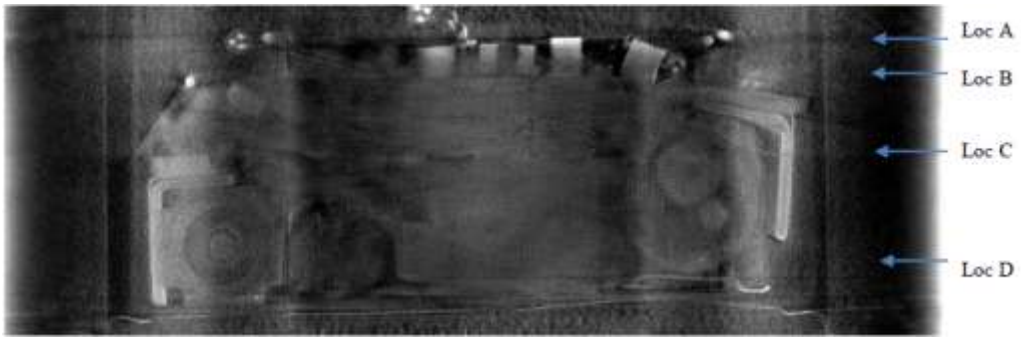

Figure 11 – Vertical slice through the High-Density

The CT inspection volume shown in the above figure of the cone-beam reconstruction for the section, includes regions with reasonable detail, and regions where the artifacts obscure the features of the contents. The cross-sectional slices at the positions in the figure show this in some detail.

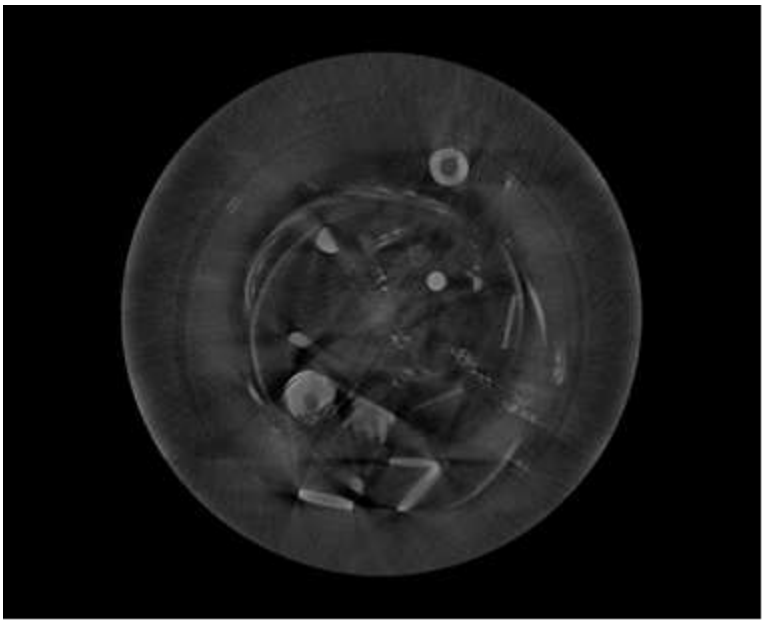

Figure 12 – Cross-Sectional Slice at Location A

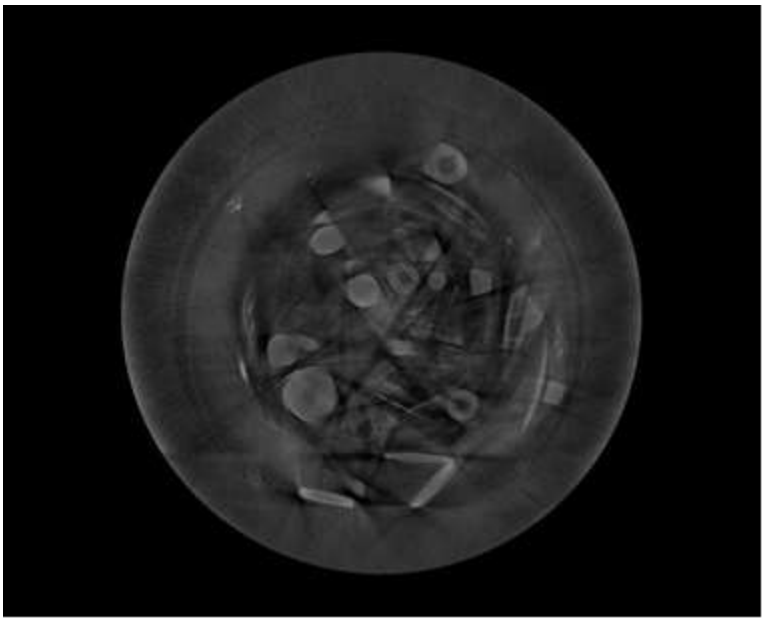

Figure 13 – Cross-Sectional slice at Location B

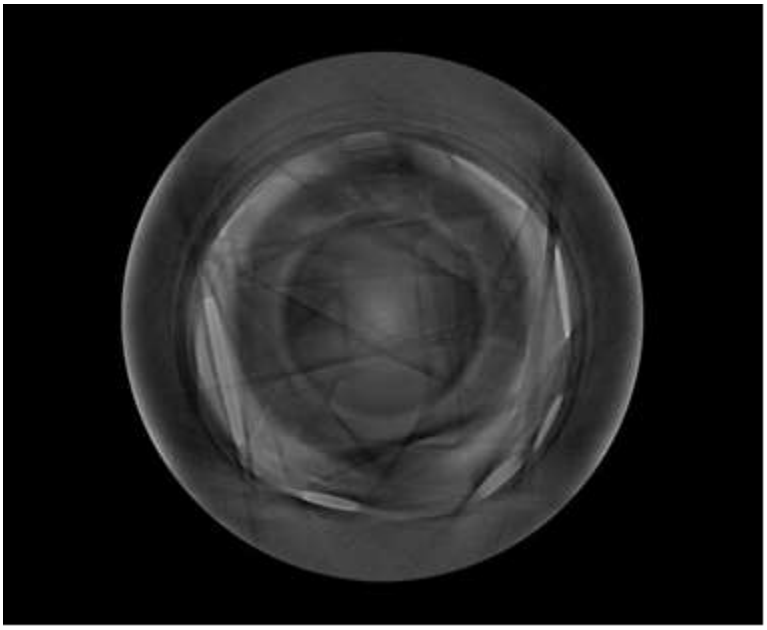

Figure 14 – Cross-Sectional Slice at Location C

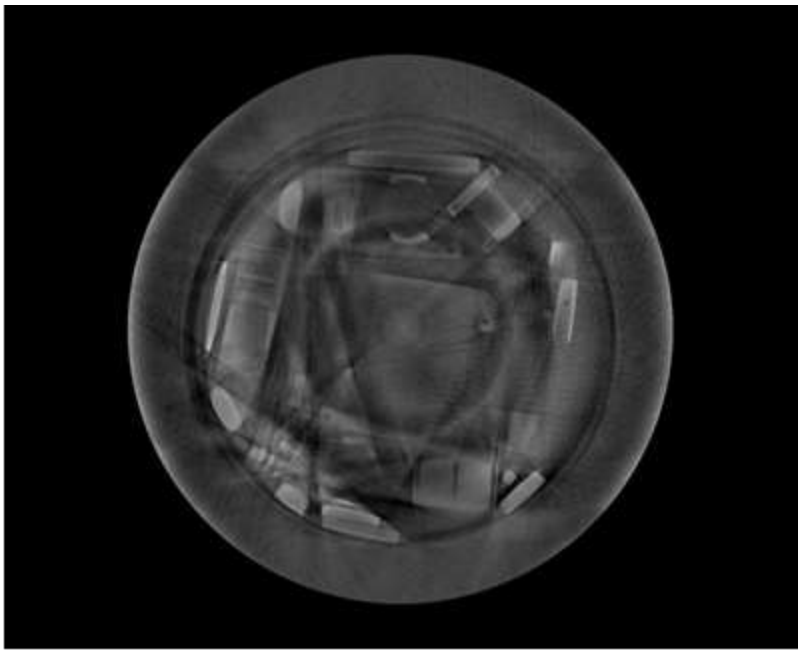

Figure 15 – Cross-Sectional Slice at Location D

Range-Extension CT scanning with the Digital Detector Array enabled coverage of a substantial section of the High-Density section of the 200 liter drum. In locations where more of the beam transmitted through the drum (locations A, B and D) full 3D detail of drum contents was imaged. However in the middle of the High Density drum the meager transmission combined with the low stopping-power of the detector resulted in a distinct lack of detail in the middle of the image.

The CT reconstructed volume has a number of artifacts. The circular artifacts in this reconstructed volume are attributed to a mismatch between the modeled version of the 'Reference Irradiance', that is the detected irradiance on the detector with no part or concrete in the field of view. Included in the processing is an 'adjustment' to the 'Reference Irradiance' for the horizontal positions of the detector, and the boundaries of the circular artifacts correspond to the position of the detector for the different translate-rotate positions.

The streaks across the images in the high-density section are considered to be a result of the meager stopping power of the detector.

The total counts in any one of the pixels in the PE panel is the sum of primary, scatter-from-object, scatter-from-detector, scatter-from-room/collimator and digitization noise. The CT reconstruction routine treats all of these photons as primary. Since at some angles of rotation there are very few of the primaries, photons in the 3MeV range that include information about the object, but at other angles there are sufficient photons, the reconstruction routine distributes the attenuation to the locations which have no primaries. This results in streaks.

Figure 16 shows a vertical slice through the low density waste, with two locations identified as A and B. Horizontal slices at each location are shown in Figures 17 and 18.

Low density part of the drum

Regarding the superior part with low density objects, we think that the detector is not thick enough to detect correctly the 9 MeV photons of the accelerator at the center of the drum.

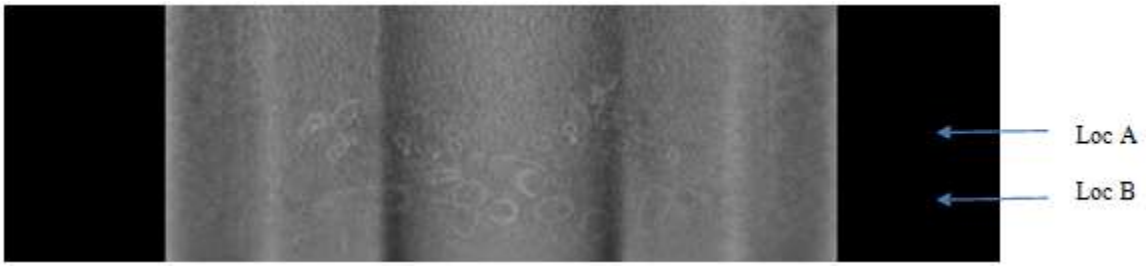

Figure 16 – Vertical slice through Low-Density section

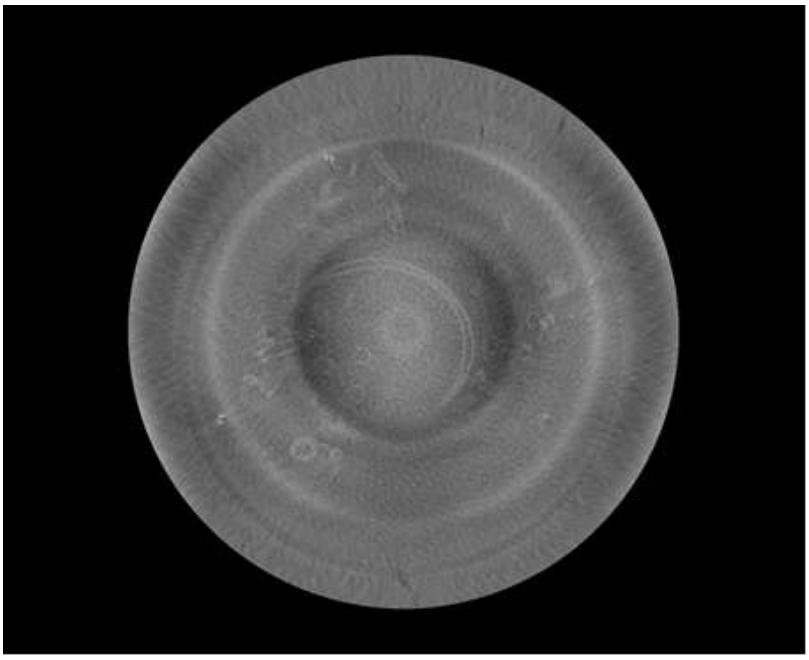

Figure 17 – Cross-Sectional slice at location A

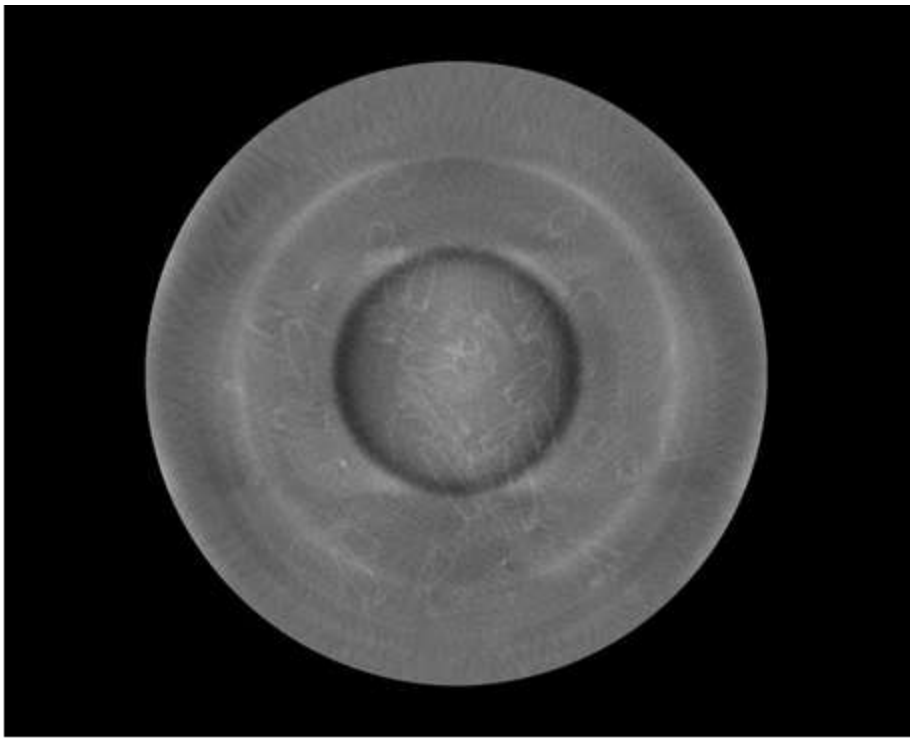

Figure 18 – Cross-sectional slice at Location B

The CT inspection volume for the low-density section shows the presence of the small-low- attenuating objects in the Inner drum. At this point the artifact content and the signal-to-noise combine to mask the presence of the low attenuating foam pieces, and the gloves and paint masks. Only the glass-bottles are imaged in the CT reconstructed data. As expected the attenuation values for the low attenuating objects are small compared with the items in the higher density sections of the drum. Also, the more significant artifacts are on par with the attenuation values of the low density objects. Alternatively, notice the lack of streaking in this volumetric data, indicating the streaks are related to the presence of higher-attenuating objects in the high-density drum. As indicated above we consider this a result of the lower-stopping power of the CsITl scintillator included in this detector. Also, as indicated in the previous section there are the circular artifacts as a result of a mismatch between the estimates of the 'reference irradiance' and the actual irradiance.

TOMOGRAPHY WITH THE LINEAR DETECTOR

Figure 19 illustrates the scanning geometry used for acquiring CT data with the Linear Diode Array (LDA) detector, using the fan-beam – rotation-only scanning option shown in Figure 5. The drum rotates between the source and the detector, which moves horizontally and vertically in order to cover the object.

Figure 20 illustrates the scan geometry used for the LDA.

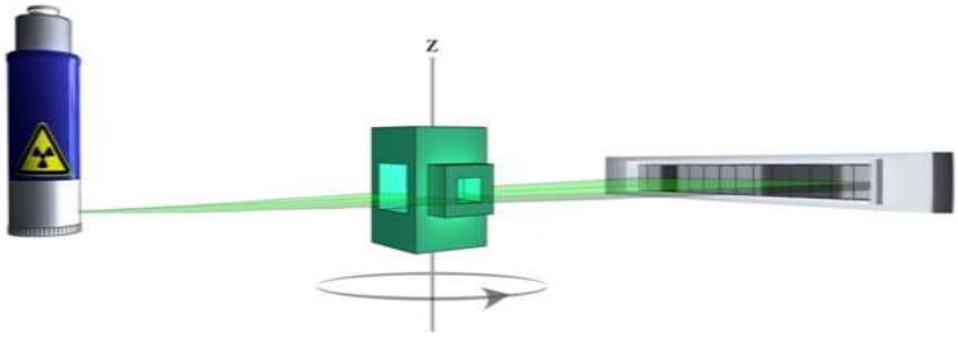

Figure 19 – Illustration of the fan-beam geometry used to scan the Concrete-Cask with the LDA detector

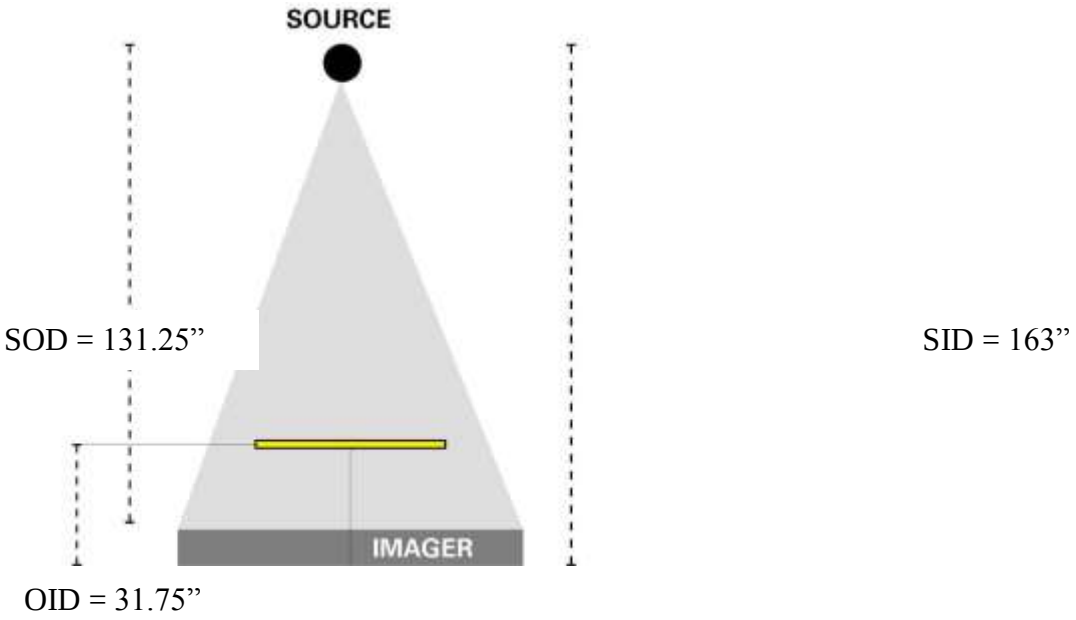

Figure 20 – LDA Scan geometry

LDA scans were acquired with 9MeV x-ray spectra, operated at a trigger rate of 300 Hz.

The width of the LDA detector is equivalent to the width of the area detector (1024 * 0.4 = 409.6 mm = 2048 * 0.2mm). As for the area detector CT Range extension techniques were used to image the 200 liter drum. With the LDA a single centered ROI scan, and ROI scans in the “offset” configuration were performed.

Figure 21 shows the concepts employed for the LDA scanning (a reprint of the top sketches Figure 5).

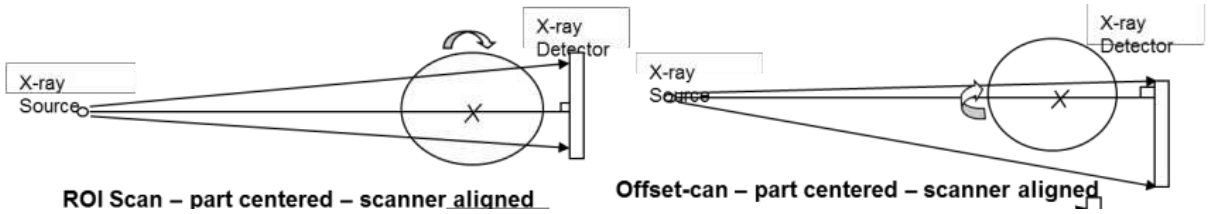

Figure 21 –ROI scanning and Offset-scanning used in the LDA

The result for the LDA scanning configuration was a slightly smaller reconstructed volume but generated from one acquisition of the detector. Offset-scanning requires less input data for the reconstruction and has proportionately higher noise relative to a complete scan. However, the higher stopping power of the LDA detector more than compensates compared to the scan with the area detector. The LDA technique scans a single cross-sectional slice, which makes scanning at exactly the same position as the area detector difficult to achieve. As a result the LDA scanning covered slightly different regions of the 200 liter drum.

Both the centered and the offset scanning were ROI scans, and the detector did not cover the outside edge of the Concrete Cask. A known artifact in the reconstructed image will result in a brighter ring around the outside of the reconstruction sphere, a circle in the case of one line on an LDA. This occurs due to the mass of the outside of the concrete container that is in projections as the image is acquired through both walls of the Concrete Cask, and is left to build up on the outside of the reconstruction sphere due to the smaller reconstructed region. An ROI correction to these data was used.

To scan the contents of the 200 liter drum requires the outer walls of the concrete, which are in every projection, to be penetrated, but for Region of Interest scanning only the contents of the 200 liter drum are reconstructed. In this circumstance we have violated the "finite extent" assumption for CT reconstruction algorithms. As a result, CT reconstruction algorithms put the mass of the outer walls on the outside of the reconstruction sphere, resulting in a sharp cupping artifact from outside to inside of the reconstruction. Since the Concrete container is a cylinder the artifact, which is quite symmetrical and can be subtracted out and the reconstructed image.

CT acquisitions were performed using four inspection configurations.

First inspection configuration.
The first inspection was centered on the middle of the drum, at a height corresponding to the medium density part in the 200liter drum.

The first scan was a centered scan with the center of the x-ray beam in the center of the detector and the detector covering the inner section of the 200 liter drum. Consequently, the reconstructed volume was restricted to the inner volume of 330mm in width.

The results are shown in Figure 22.

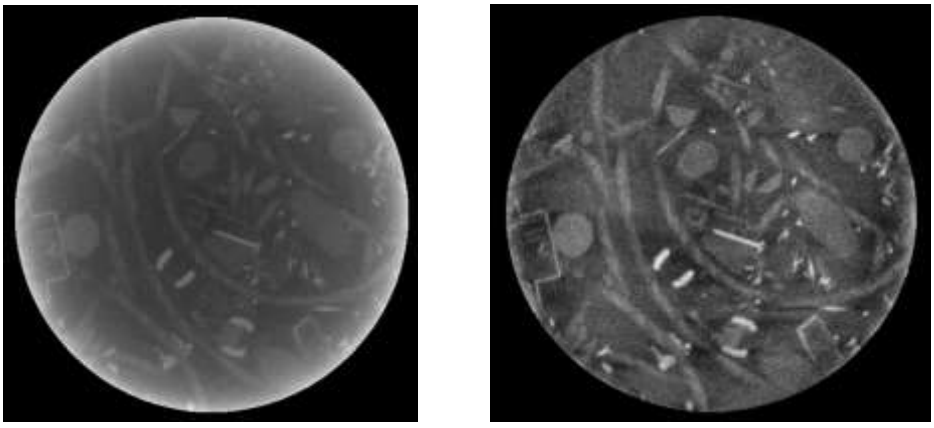

Reconstruction from Centered Scan ROI Correction Applied

Figure 22 – Cross-Sectional slice from Centered scan with and without ROI Correction.

Second inspection configuration.
The second scan was a shifted acquisition in the middle of the drum, at a height which corresponds to the medium density part in the 200 liter drum.

The offset scan was acquired with the perpendicular to the center of rotation approximately 12mm from end of the detector. Using this configuration and magnification the image was reconstructed into a field of view of approximately 600mm in diameter. The results are shown in Figures 23 and 24.

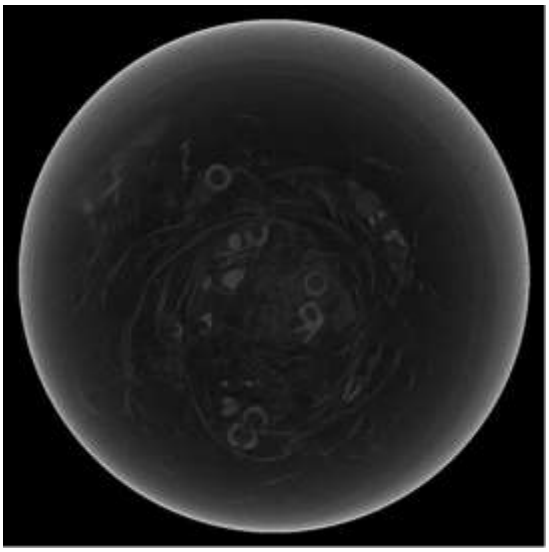

Figure 23 – Cross-Sectional slice from LDA scan through Medium Density region – No ROI Correction applied

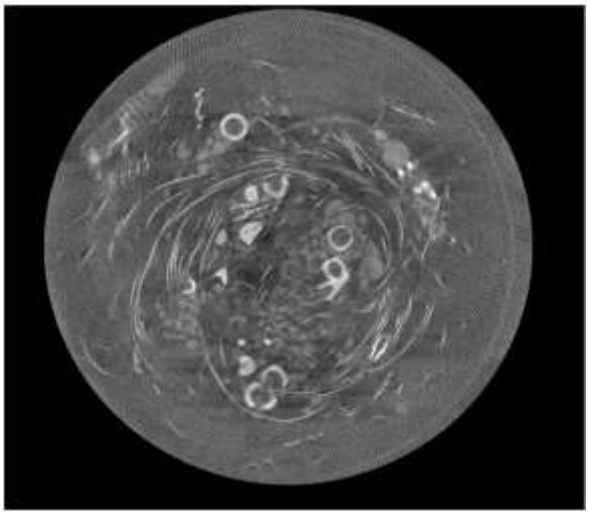

Figure 24 – Cross-Sectional slice from LDA scan through Medium Density region – ROI Correction applied

Third inspection configuration.
The third scan was an offset acquisition in the middle of the drum, at a height which corresponds to the low density part in the 200 liter drum. The results are shown in Figures 25.

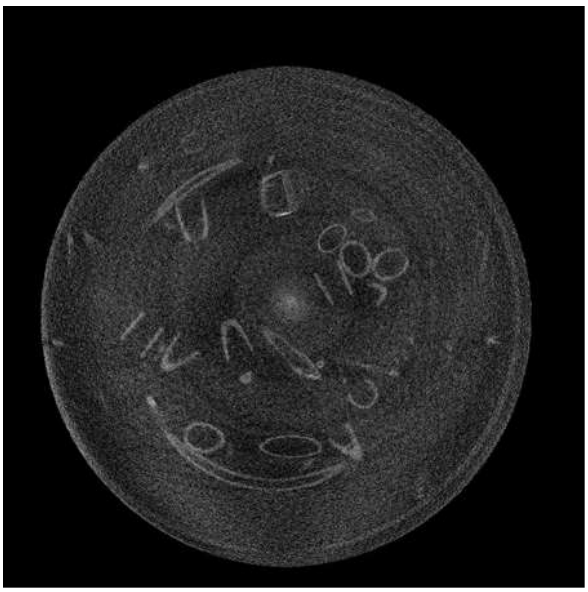

Figure 25 – Cross-Sectional slice from LDA scan through Low-Density region - ROI Correction applied

Fourth inspection configuration.
The fourth scan was an offset acquisition in the middle of the drum, at a height which corresponds to the high density part in the 200 liter drum. The results are shown in Figures 26.

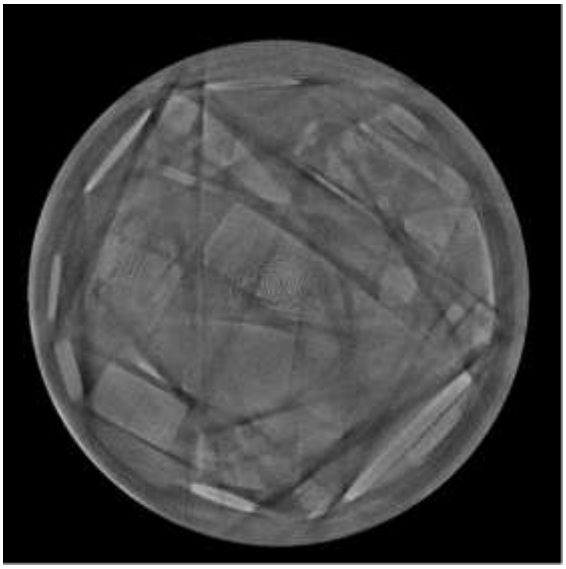

Figure 26 – Cross-Sectional slice from LDA scan through High-Density region - ROI Correction applied (pattern noise in the center of the scan from detector)

Some of the streak-features are present showing the impact of the higher attenuating materials in the high-density section of the drum. This image includes more contrast than the area detector image for the same section of the drum, but the added attenuation in the thicker sections of the 200 liter drum remains a challenge for this thicker detector.

All the scans, except the one corresponding to the high density part in the drum, produced acceptable tomographic reconstructions.

The results from the LDA scans were considered to show the following:

1. The added stopping power of the LDA resulted in clearer imaging of the 200 liter drum contents for the low-density and medium-density sections.
2. This added detail on the 200 liter drum was present for both Centered-ROI scans and Offset- ROI scans. Both of these scans were acquired with a single acquisition demonstrating the utility of the ROI approach to scanning the 200 liter drum.
3. A first-cut ROI correction was able to remediate the expected artifacts for ROI scanning.
4. In spite of the added stopping power the high-density scan included some of the same artifacts found in the scans with the area detector.

5. The LDA detector developed some digitization artifacts over the course of scanning. This was considered to be detector failure.

TOMODENSITOMETRY

The tomographic quality of the images prevented full and complete density interpretation. However, certain information was extracted from a slice of average density materials, and described as follows:

High Z materials are identified at 0.008 mm-1 or better.
Lower density materials at 0.006 mm-1.

The combination of the Concrete Cask and the materials in the 200 liter drum constitute substantial attenuation for the 9 MeV LINAC spectrum. The result is the differences between materials should scale with the expected attenuation differences of materials at approximately 2-3 MeV. Referring to Table 1, the measured attenuation in Steel parts is expected to be over twice that of Aluminum and Concrete, and 4 to 5 times higher than plastic. It is considered that obtaining material differences with this scaling represents the best achievable at 9MeV in this imaging context. This represents the differences in materials in the object, irrespective of the detector or the scanning technique.

The scans from both the area detector and the LDA did not include robust detail for the center of the High-Density section of the 200 liter drum. However, the scans from both detectors included interesting detail on both the Medium-Density region of the 200 liter drum and the Low-Density region of the 200 liter drum. Since there was little material difference in the low-density section of the drum, attention was focused on the medium-density sections of the 200 liter drum.

The basis for materials identification from CT scan data is simply the differences in the values of the voxels in the reconstructed volume. While there are a number of options for improving performance for materials identification; analytic continuation and 'Statistical Reconstruction' for generating the CT volume, and different approaches to 3D segmentation on the entire volume, all of the approaches begin with contrastive differences between these materials at this energy with the detectors available.

Therefore, the potential for materials identification from these scans from an inspection of the voxel values was evaluated. Three aspects of the voxel values are important; 1) the size of the difference between the voxel values for different materials, 2) the overall level of the image noise, and 3) the size of the artifacts in the scans. The units of the reconstructed images are in mm-1, with the ROI Correction applied.

Figure 27 shows the materials in the top section of the Medium-Density section of the drum for reference.

Figure 27 – Materials in the top section of the Medium Density section

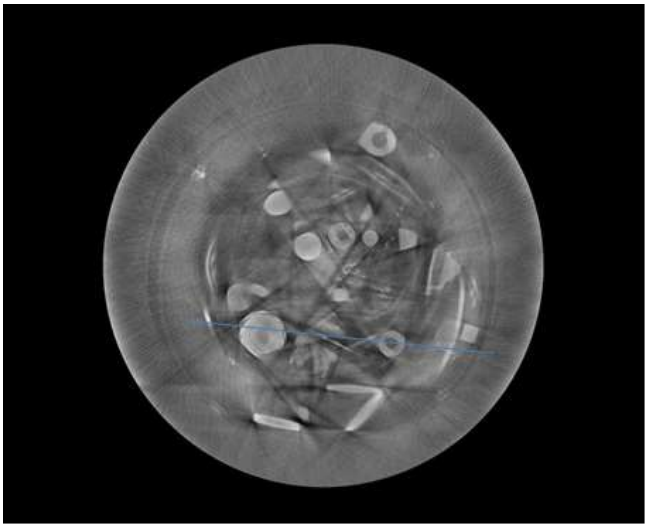

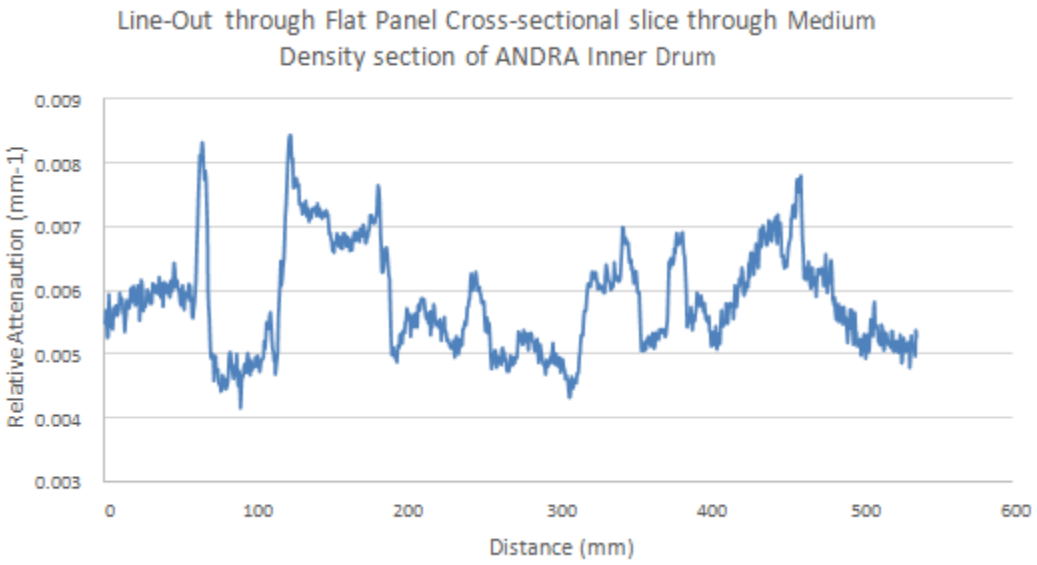

Figure 28 – Cross-sectional slice through Medium-Density section of Inner Drum and Line- out from image showing differences in measured material values from the Digital Detector Array (Area Detector) CT data.

The area detector volumetric data plotted from the line-out covers a roll of lead, two carbon-steel parts, and some copper wire. The attenuation value of the lead is a little higher than the steel and copper materials, but the voxel-value differences are low, and the noise is considerable.

Figures 29 and 30 show a cross-sectional slice from the LDA offset-scan of the medium-energy section of the Inner test drum, the voxel-values from the LDA acquisition and a line-out showing the voxel values from a line-out taken from the middle of the volumetric image.

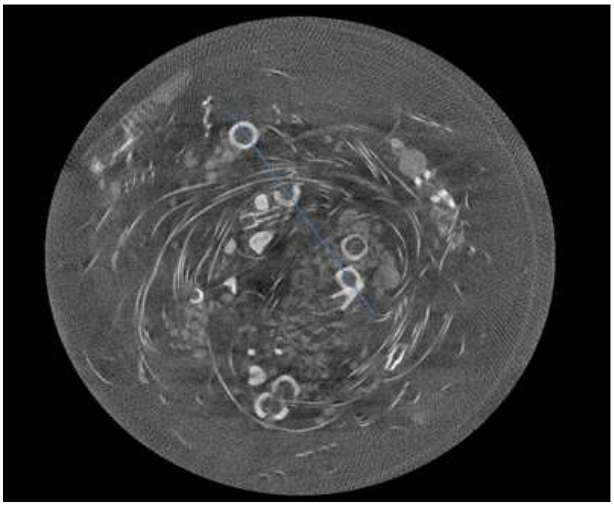

Figure 30 – Cross-sectional slice through the medium density section of the Inner Drum, with the position of the Line-out plot indicated on the image

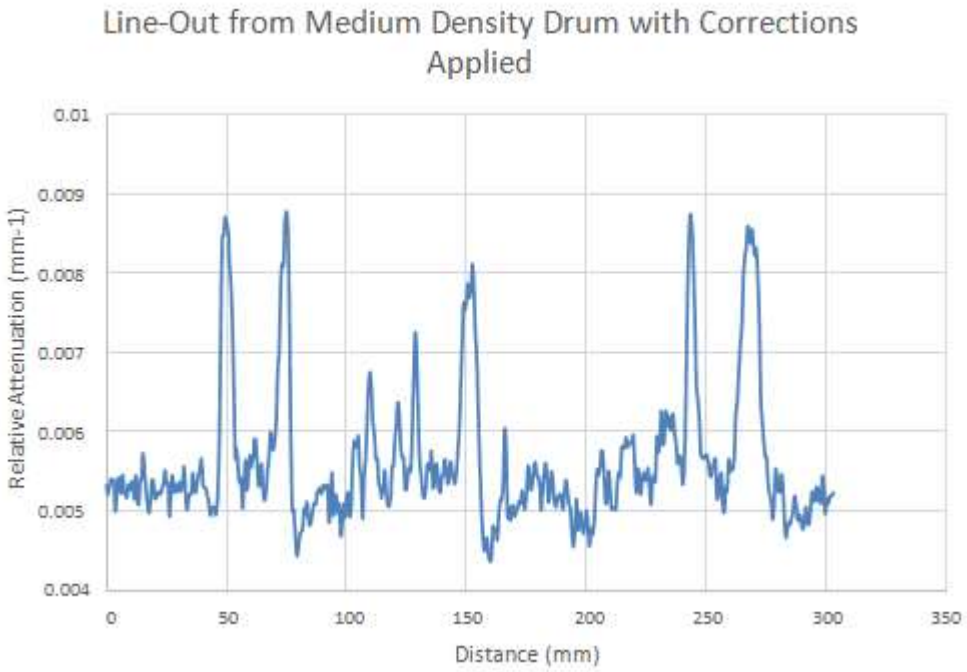

Figure 31 – Cross-sectional slice through Medium-Density section of Inner Drum and Line- out from image showing differences in measured material values from the LDA CT data.

The voxel-values obtained from Line-out through the data from the LDA shows more fidelity for materials discrimination. The line-out traverses, a brass part, then steel, then gravel, then brass. The brass is higher in voxel value than the steel, and the gravel. Also, the double-peaks at the start and the end of the line-out nearly match in voxel value, indicating this scan measures the value of brass similarly regardless of its position in the volumetric data.

Both the Digital Detector Array and the LDA CT scan data distinguishes materials by voxel value. In both cases the line-outs show that the higher density materials include a higher measured attenuation value. While the absolute scale is bound somewhat by the ROI correction, the differences between the two different types of scans are important. First, and as expected, the LDA is cleaner, the steel and copper components are distinctively higher than the surrounding materials, and from the line-out are far above any local noise variation. Second, while the Digital Detector Array cross-sectional slice includes more noise, the artifacts also detract from the measured differences in the CT data. The Digital Detector Array data includes a bit of a "cupping" artifact which impacts the value of the CT voxels dependent on position not on the material. Second, the overall difference in measured material range is smaller for the Digital Detector Array.

For both data sets, while the high-density (in this case higher-Z) materials in the medium-density section, and in the top of the high-density section were imaged crisply, the lower-Z materials were not measured with robust accuracy. In the LDA

scan, where the contrast is the best; steel, copper, brass and gravel include distinct voxel values. The differences far exceeded the local noise variation.

SUMMARY AND FURTHER RESEARCH

The overall conclusions of this work are considered to be as follows:

Digital Detector Array

1. Translate-rotate scanning can generate CT inspection volumes with considerable resolution and detail for the low-density and medium-density sections of the 200 liter drum. The high-density sections of the 200 liter drum were not imaged with sufficient detail and were inundated with artifacts.
2. The artifacts stemmed from the lack of stopping power in the detector, and from a possible mismatch with the 'modeled' reference irradiance used in the processing of the acquired radiographs. While the second source of artifacts can be remediated by more extensive calibration data, the first source requires some change in the scintillator used in the detector, or much longer scan times.
3. Materials identification with the Digital Detector Array, while possible for certain high-density materials, is difficult in any kind of automated fashion. For materials in the steel to plastic range the attenuation values of the voxels in the reconstruction are not very different, and some differences are on par with the artifact content.

LDA Detector

1. ROI scanning, and Offset-ROI scanning with the LDA detector can generate inspection volumes for the low and medium density volumes considerable resolution and contrast. While the high-density sections of the drum were not imaged well, part of the problem was connected to the digitization on the detector. Both types of ROI scanning can generate robust inspections of the 200 liter drum in a single acquisition with standard equipment.
2. The few artifacts in the LDA scans were considerably less than the artifacts in the Digital Detector Array scans. The principal artifact was a consequence of the ROI scan, which was remediated with a first-cut ROI correction.
3. Materials identification with the LDA inspection data appear to be feasible, and with these scans steel, copper, and higher-density metals can readily be distinguished from other materials on the basis of voxel value.

Future Work

1. Review and quantify operational benefits with respect to target spatial resolution and inspection speed.
2. Reduce artifacts produced by Digital Detector Arrays. This will include research using alternative scintillator materials which could be more effective at stopping high energy x-rays.
3. Reduce circular artifacts by acquisition of multiple-series of 'calibration' empty Concrete Cask scans to further refine the estimates of the 'reference irradiation' used in the scanning of drums.
4. Develop a calibration drum using cylinders/rods of a range of material densities such as plastic, teflon, concrete, aluminum, copper, tungsten and lead.
5. Investigate artifact reduction in LDA scanning.
6. Evaluate the use of Iterative reconstruction methods for High-Density Inner Drums.